Stripe Noise Reduction in MODIS Data by Combining Histogram Matching With Facet Filter

Preesan Rakwatin, Wataru Takeuchi, and Yoshifumi Yasuoka, *Senior Member, IEEE*

***Abstract*—The Moderate Resolution Imaging Spectrometer (MODIS) aboard Terra and Aqua platforms are contaminated by stripe noises. There are three types of stripe noises in MODIS data: detector-to-detector stripes, mirror side stripes, and noisy stripes. Without correction, stripe noises will cause processing errors to the other MODIS products. In this paper, a noise-reduction algorithm is developed to reduce the stripe noise effects in both Terra MODIS and Aqua MODIS data by combining a histogram-matching algorithm with an iterated weighted least-squares (WLS) facet filter. Histogram matching corrects for detector-to-detector stripes and mirror side stripes. The iterated WLS facet filter corrects for noisy stripes. The method was tested on heavily striped Terra MODIS and Aqua MODIS images. Results of Terra MODIS and Aqua MODIS data show that the proposed algorithm reduced stripes noises without degrading image quality. To evaluate performance of the proposed method, quantitative and qualitative analyses were carried out by visual inspection and quality indexes of destriped images.**

***Index Terms*—Destriping, facet model, histogram modification, image filtering, Moderate Resolution Imaging Spectrometer (MODIS).**

I. Introduction

THE MODERATE Resolution Imaging Spectroradiometer (MODIS) aboard the Earth Observing System (EOS) Terra and Aqua platforms has been designed to provide data for studies of the Earth's land, ocean, and atmosphere [1], [5], [7]. MODIS sensor has 36 spectral bands covering wavelengths in the visible, near infrared, short and midwave infrared, and long wave infrared (LWIR). It has three different nadir ground spatial resolutions: 0.25 km (band 1–2), 0.5 km (band 3–7), and 1 km (band 8–36). In the along-track direction, there are 40 detectors per band for band 1–2, 20 detectors per band for band 3–7, and 10 detectors per band for band 8–36. MODIS uses a double-sided scan mirror that views onboard calibrators and the Earth scene at 20.3 r/min. The prelaunch developed characteristics and algorithms of Terra MODIS were described in [1] and [2]. The orbit performance of Terra MODIS was presented in [3]–[7]. The information on the current performance and status of both Terra and Aqua MODIS can be checked on the MODIS homepage (http://modis.gsfc.nasa.gov) and the MODIS Characterization Support Team (MCST) homepage (http://www.ncst.ssai.biz) [6].

Since the launch of Terra and Aqua, a great deal of work has been performed to assess MODIS data quality. Even though MCST MODIS L1B calibration algorithm can effectively handle operational artifacts like optical and electronic crosstalk, shortwave infrared thermal leak, etc. [3], [6], [20], stripe noise still remains in the images. Without stripe noise correction, this noise will degrade the image quality and introduce a considerable level of noise when the data are processed. Gumley [8] mentioned that MODIS data have three kinds of stripe noises which are detector-to-detector stripes, mirror side stripes (banding), and noisy stripes.

A detector-to-detector stripe is characterized by a pattern of sharp, repetitive stripes over entire images [13]. According to [11], [13], and [23], the reason of detector-to-detector striping is mainly caused by relative gain and/or offset differences among detectors within a band. Another reason is that photomultipliers are nonlinear and have a response which depends on their exposure history [26].

Mirror side stripe (banding) is a sudden change of bias level of all detectors. The change occurs during the scan mirror's turnaround, and the amount of change is quite constant [27]. The image appearance is slightly brighter and darker scans (clearly seen in homogeneous areas such as oceans) [28]. The source of MODIS mirror side stripes is a difference in offset between the forward and reverse scan calibrations [27]. Another source of mirror side stripes is "bright target overshoot" or "bright target saturation." This occurs when detectors are scanned across a highly reflective target, such as clouds or snow cover, followed by a sharp transition to a region of lower reflectance. Detector overshoot causes scans to be darker than adjacent scans [27]. In some cases, mirror side stripes also correlate with scan angle, particularly in the images of LWIR bands (MODIS band 33–36).

Noisy stripes are caused by slight errors in the internal calibration system, variation in the response of the detectors, and random noise [12], [21], [24]. Noisy stripes in MODIS data mostly occur in the thermal band and is getting worse over time. For example, a progressive deterioration of the Terra MODIS band 28 is obviously seen in Fig. 1. The image from April 27, 2003 [shown in Fig. 1(a)] provides a rather different character of interference observed from the image taken on September 16, 2004 [Fig. 1(b)].

Manuscript received July 1, 2006; revised December 4, 2006. This work was supported by the Japan Science and Technology Agency under the research project "Solution Oriented Research for Science and Technology (SORST)."

The authors are with the Institute of Industrial Science, University of Tokyo, Tokyo 153-8505, Japan (e-mail: preesan@iis.u-tokyo.ac.jp).

Digital Object Identifier 10.1109/TGRS.2007.895841

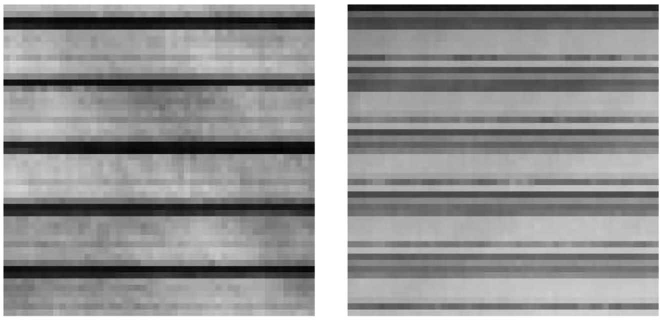

(a) (b)

Fig. 1. Terra MODIS band 28 subimages over a homogeneous region. Image size is 200 × 200 pixels. Images were taken on (a) April 27, 2003, and (b) September 16, 2004.

Even though there are several methods to correct stripe noise in satellite data, a few of them can correct a stripe due to random noise. In this paper, a destriping algorithm was developed by combining histogram matching with an iterated weighted least-squares (WLS) facet filter to correct striping errors which are presented in Terra MODIS and Aqua MODIS images. Histogram matching is used to correct detector-to-detector stripes and mirror side stripes, while iterated WLS facet filtering is used to remove the random noise of noisy stripes. Although the proposed method shows the improvement of the image quality, it is not meant to provide a radiometric correction. For this reason, it may create some problems when applied to band data that will be used in numerical analysis.

This paper is organized as follows. Section II describes previous destriping methods. Then, Section III introduces a MODIS destriping procedure using histogram matching and iterated WLS facet filtering. The data processing is discussed in Section IV and its experimental results and quantitative evaluation of both Terra MODIS and Aqua MODIS images shown in Section V. Finally, Section VI is a summarization and conclusion of this research.

II. Previous Destriping Algorithm

There are three major approaches developed for removing detector-to-detector stripes and mirror-side stripes (banding) in satellite images. The first approach is to construct a filter for removing stripe noise at a given frequency [9]–[15]. This algorithm follows the fact that stripe noise is periodic and can be identified in the power spectrum [15]. This method has the advantage of being usable on georectified images, and on smaller images than the other approaches [15], [22]. However, this filter does not only suppress part of the spatial frequency component which is produced by stripe noise, but also affects part of the same component which is caused by the image generation process [22], [26]. It also has more or less the effect of ringing artifacts at the point where radiances change abruptly, such as coastlines [15], [22].

The second approach is wavelet analysis, which has been recently applied to remove stripe noise [16]–[18]. Wavelet analysis takes advantage of the scaling and directional properties to detect and eliminate striping patterns in the wavelet domain [16]. However, this technique has more or less smoothing of the image. The destriping effect of this method depends on the selection of a wavelet transform function and location of frequency components produced by stripes [18].

Third approach examines the distribution of digital numbers (DNs) for each sensor, and adjusts this distribution to some reference distribution [22]. This assumes that each sensor will view a statistically similar subimage. Unlike the first approach, this approach cannot be applied to the georectified data. These methods are equalization [19]–[21], moment matching [22], and histogram matching [23]–[26].

Equalization was applied to remove nonperiodic striping in NOAA-3 and NOAA-4 satellite data [21]. However, this method does not account for nonlinearity in detector variation [9]. Corsini *et al.* [19] processed a training set of MOS-B satellite images to estimate the equalization curve to correct stripe noise. It is based on the assumption that a striping entity does not vary with time, and targets in the image area are homogeneous or quasi-homogeneous [15], [20].

The moment-matching algorithm is based on the assumption that means and standard deviations of data recorded by any of the sensors will not differ significantly [20]. This assumption is invalid if an object boundary runs nearly parallel to a scan line and an object is too small to be imaged by all detectors within a given sweep [13], [15], [26]. Moment matching has its advantage in avoiding the introduction of binning errors because it calculates adjusted DNs using real numbers, which are then rounded [22].

Histogram matching matches the histogram of uncalibrated data to the reference data [9]. This method is easy to implement and gives fast processing. However, the histogram-matching method is scene dependent [13], [14] and requires the specification of reference data which may change with time [14].

III. Methodology

A. Histogram Matching

The histogram-matching algorithm assumes that with a large scene, the distribution of the intensity of Earth radiation incident on each detector will be similar [23].

Histogram matching maps the cumulative distribution function (CDF) of each detector to a reference CDF. A normalization lookup table is created for each detector to map every DN x to a referenced DN x'. If $p_i(x)$ is the histogram of output of the ith detector, the CDF of ith detector $P_i(x)$ is

$$P_i(x) = \sum_{t=0}^{x} p_i(t). \tag{1}$$

CDF is a nondecreasing function of x, and its maximum value is unity. The basic assumption is that the CDF of each detector is a monotonic function. For each output value x of the ith detector, the value x' should satisfy

$$P_r(x') = P_i(x) \tag{2}$$

where the subscript r refers to the reference detector. Therefore, a modified DN x' can be obtained from

$$x' = P_r^{-1}\left(P_i(x)\right). \tag{3}$$

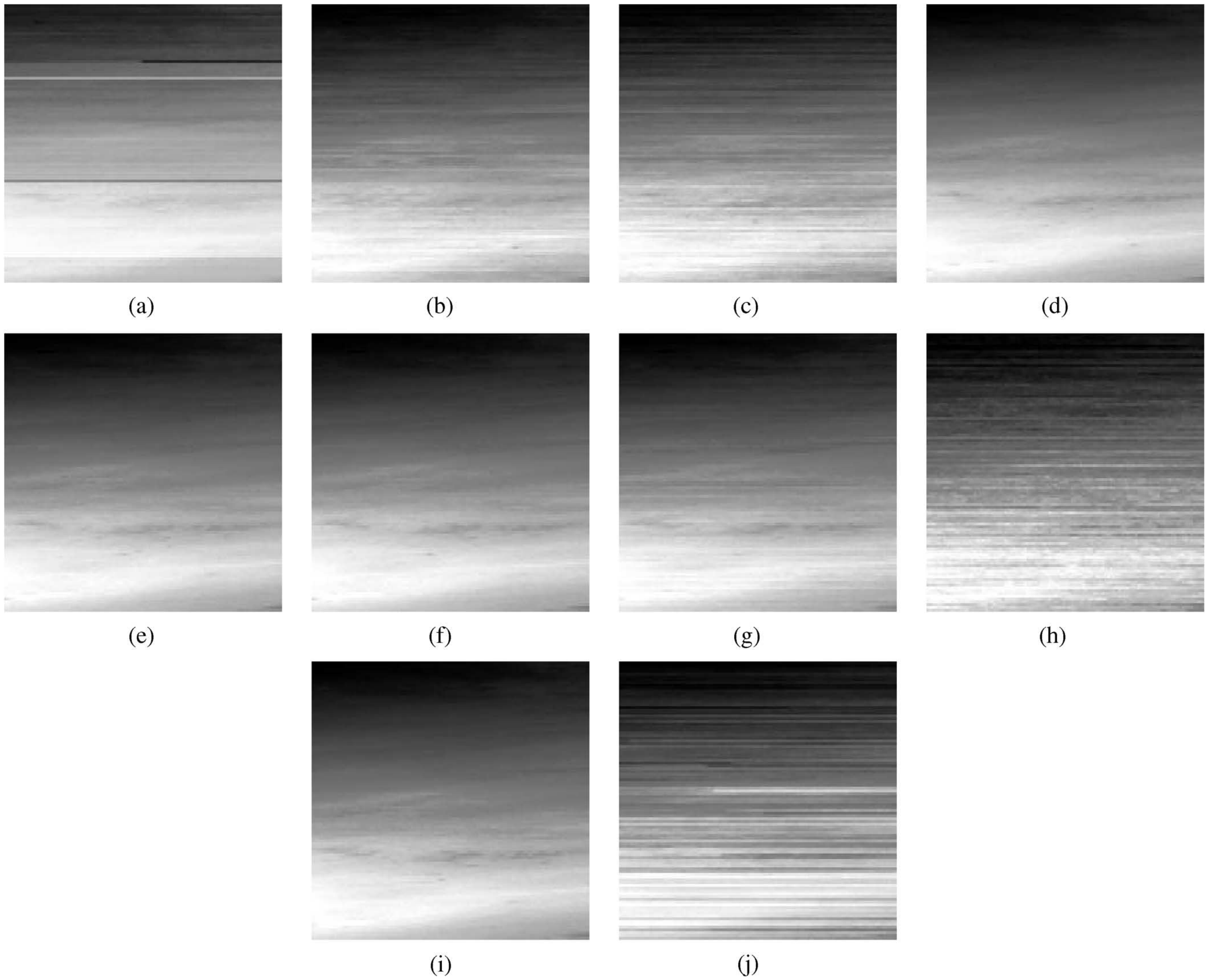

Fig. 2. Ten detector subimages separated from Terra MODIS band 28 taken on September 16, 2004. Each detector subimage has 200 × 200 pixels. (a)–(j) First to tenth detector subimages, respectively.

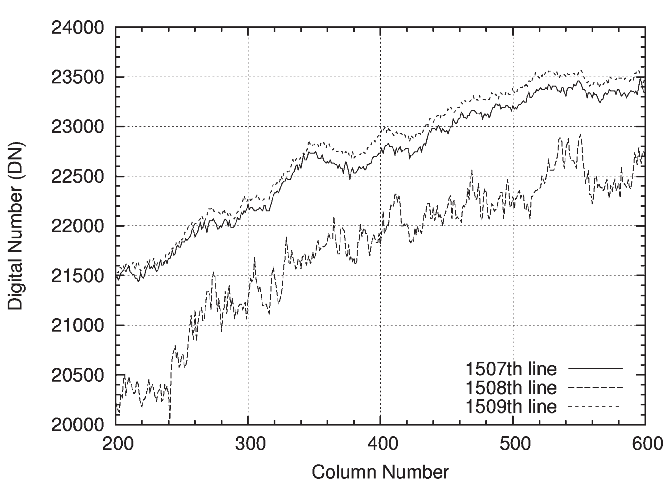

Fig. 3. Sample plot of the along columns data extracted from Terra MODIS band 28 before destriping. Image was taken on September 16, 2004.

Histogram matching has successfully been applied to satellite data such as the Landsat Multispectral Scanner [23], Landsat Thematic Mapper [24], and Geostationary Operational

TABLE I
MODIS BANDS AND THEIR NOISY DETECTORS OF TERRA MODIS IMAGES TAKEN ON SEPTEMBER 16, 2004, AND AQUA MODIS IMAGES TAKEN ON NOVEMBER 5, 2005

Band	Wavelength (μm)	Defected Detector (1st-10th)
Terra B27	6.715	1st, 2nd, 4th, 6th, 7th, 8th
Terra B28	7.325	1st, 2nd, 3rd, 7th, 8th, 10th
Terra B30	9.730	5th, 8th
Terra B33	13.335	1st
Terra B34	13.635	6th, 7th, 8th
Aqua B27	6.715	3rd
Aqua B36	14.235	5th

Environmental Satellite [25]. However, striping is still presented in some cases after histogram matching. This is because the subimages' CDF are quite substantially different. This disagrees with the similarity assumption. Wegener [26] introduced an additional step which attempts to ensure that sensor statistics are only calculated over homogeneous image regions. For this

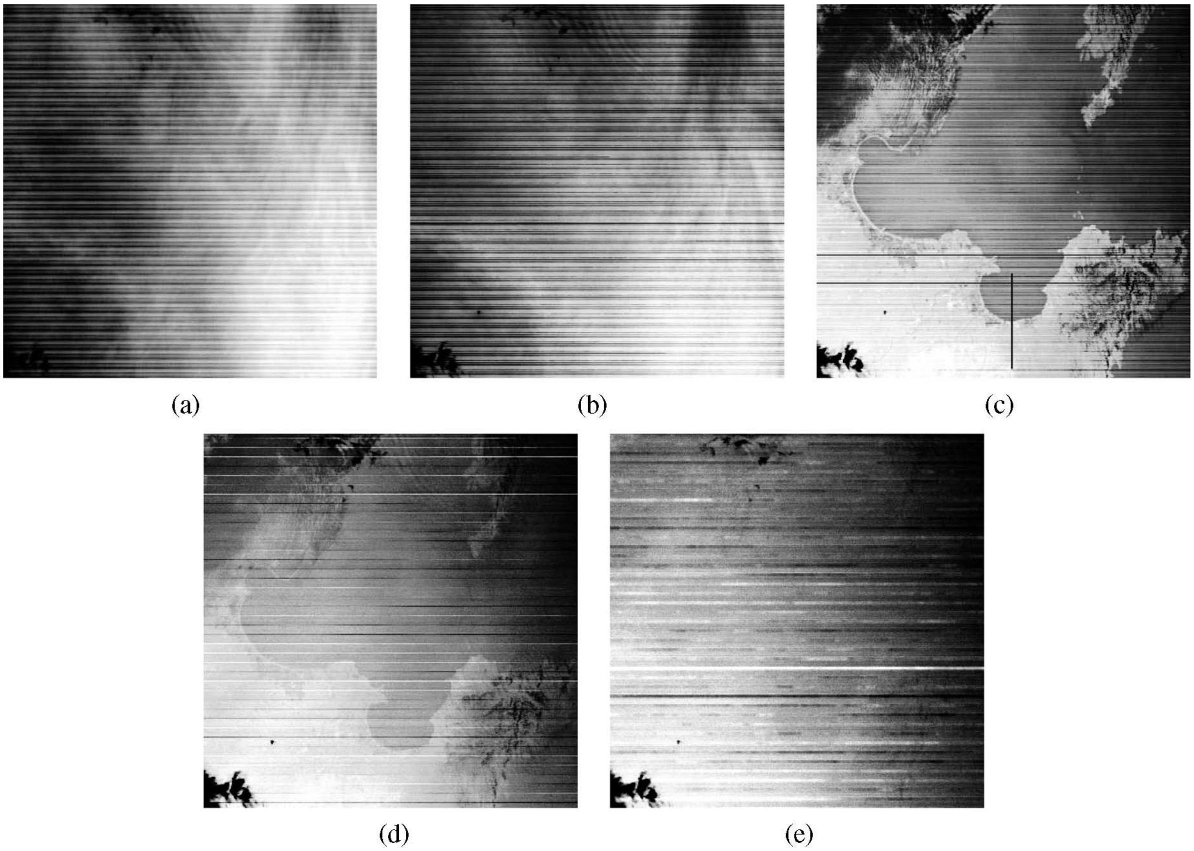

Fig. 4. Terra MODIS subimage of gulf of Chihli, Tianjin, China, showing stripe noises. The size of these images is 400 × 400 pixels (400 × 400 km). The scene was taken on September 16, 2004. (a) Band 27, (b) band 28, (c) band 30, (d) band 33, and (e) band 34.

purpose, an image was divided into small subimages. To be regarded as homogeneous, a subimage has to satisfy the testing of Bienaymè's inequality

$$P\left(|x-\mu| > k\sigma\right) < k^{-2} \tag{4}$$

where μ and σ are the mean value and variance of a subimage. Wegener [26] arbitrarily chose the critical value to be four standard deviations $(k = 4)$ on either side of the mean which give a false alarm rate of 6.25%.

B. Iterated WLS Facet Estimation

Iterated facet model for filtering was proposed by Haralick *et al.* [29] and [30]. The iterated model for image data assumes that an image can be partitioned into connected regions called facets. Each facet in the image can be represented as a union of a $K \times K$ block of pixels.

For each pixel i, a resolution cell W_{ik} is a group of neighboring pixels where $k = \{1, \ldots, K \times K\}$. Resolution cells overlap with each other; thus, each pixel is contained in more than one resolution cell [31]. If a sloped facet model is assumed for any resolution cell W_{ik}, the gray value of any pixel inside W_{ik} is assumed to obey

$$\hat{g}_{ik}(r, c) = \alpha_{ik} r + \beta_{ik} c + \gamma_{ik} \tag{5}$$

where r and c are the indexes corresponding to the row and column of each resolution cell; α_{ik}, β_{ik}, and γ_{ik} are the slope plane coefficients for each W_{ik}.

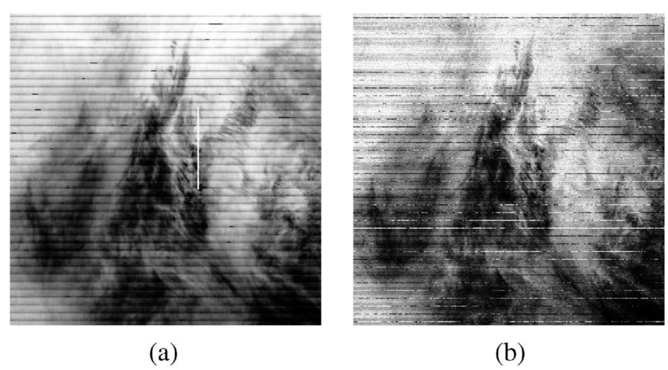

Fig. 5. Aqua MODIS subimage of Pacific Ocean, near Tohoku area, Japan showing stripe noise. The size of these images is 400 × 400 pixels (400 × 400 km). The scene was taken on November 5, 2005. (a) Band 27 and (b) band 36.

For each resolution cell W_{ik}, the symmetric rectangular region is assumed with odd number of block length. Let the upper left-hand corner of each cell have relative row–column coordinates $(-L, -L)$ and the lower right-hand corner have relative row–column coordinates (L, L). α_{ik}, β_{ik}, γ_{ik} of each cell are estimated from least-squares procedure

$$f(\alpha_{ik}, \beta_{ik}, \gamma_{ik}) = \sum_{r=-L}^{L} \sum_{c=-L}^{L} \left(\alpha_{ik} r + \beta_{ik} c + \gamma_{ik} - g_{ik}(r, c)\right)^2 \tag{6}$$

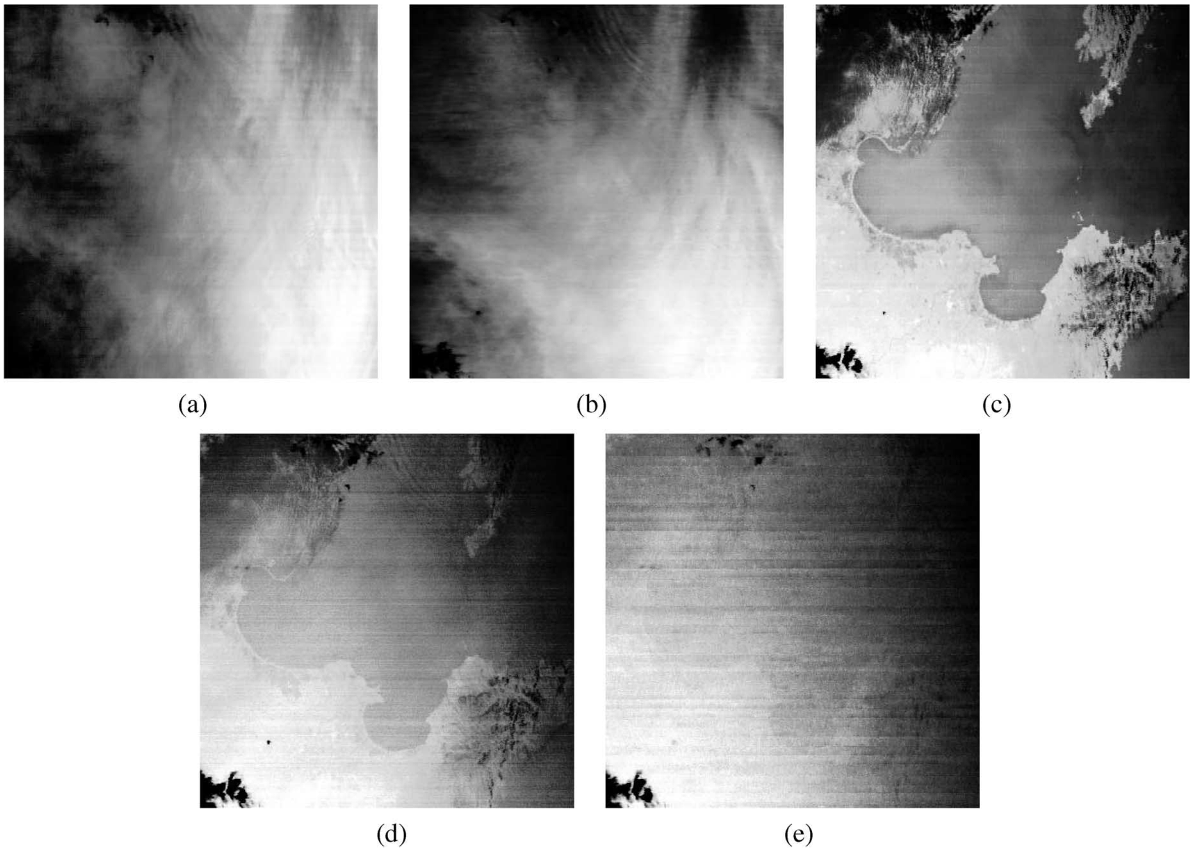

Fig. 6. Analogous to Fig. 4, except after destriping.

where g_{ik} is the gray value at row r and column c of the observed image.

To determine these values, partial derivatives of ρ_{ik} was taken with respect to α_{ik}, β_{ik}, and γ_{ik}

$$\frac{df}{d\alpha_{ik}} = 2\sum_{r=-L}^{L}\sum_{c=-L}^{L}\left(\alpha_{ik}r + \beta_{ik}c + \gamma_{ik} - g_{ik}(r,c)\right)r \quad (7)$$

$$\frac{df}{d\beta_{ik}} = 2\sum_{r=-L}^{L}\sum_{c=-L}^{L}\left(\alpha_{ik}r + \beta_{ik}c + \gamma_{ik} - g_{ik}(r,c)\right)c \quad (8)$$

$$\frac{df}{d\gamma_{ik}} = 2\sum_{r=-L}^{L}\sum_{c=-L}^{L}\left(\alpha_{ik}r + \beta_{ik}c + \gamma_{ik} - g_{ik}(r,c)\right). \quad (9)$$

Setting the partial derivatives to zero results in

$$\sum_{r=-L}^{L}\sum_{c=-L}^{L}\left(\alpha_{ik}r^2 + \beta_{ik}rc + \gamma_{ik}r - g_{ik}(r,c)r\right) = 0 \quad (10)$$

$$\sum_{r=-L}^{L}\sum_{c=-L}^{L}\left(\alpha_{ik}rc + \beta_{ik}c^2 + \gamma_{ik}c - g_{ik}(r,c)c\right) = 0 \quad (11)$$

$$\sum_{r=-L}^{L}\sum_{c=-L}^{L}\left(\alpha_{ik}r + \beta_{ik}c + \gamma_{ik} - g_{ik}(r,c)\right) = 0. \quad (12)$$

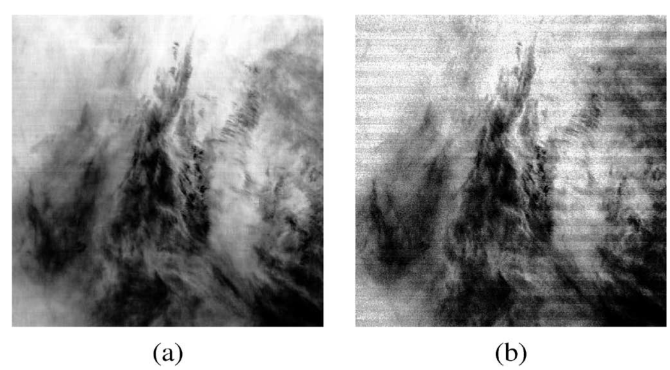

Fig. 7. Analogous to Fig. 5, except after destriping.

Using the facts that $\sum_{i=-K}^{K} i = 0$ and $\sum_{i=-K}^{K} i^2 = (1/3)K(K+1)(2K+1)$, we obtain

$$\frac{1}{3}L(L+1)(2L+1)^2\alpha_{ik} - \sum_{r=-L}^{L} r \sum_{c=-L}^{L} g_{ik}(r,c) = 0 \quad (13)$$

$$\frac{1}{3}L(L+1)(2L+1)^2\beta_{ik} - \sum_{c=-L}^{L} c \sum_{r=-L}^{L} g_{ik}(r,c) = 0 \quad (14)$$

$$(2L+1)^2\gamma_{ik} - \sum_{r=-L}^{L}\sum_{c=-L}^{L} g_{ik}(r,c) = 0. \quad (15)$$

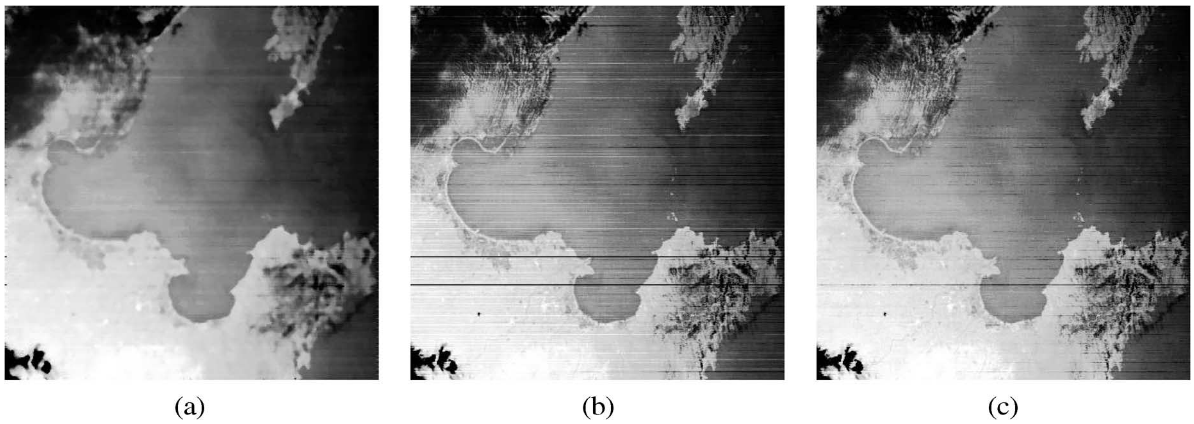

Fig. 8. Subimages of Terra MODIS band 30 destriped by (a) low pass filter, (b) moment matching, and (c) histogram matching.

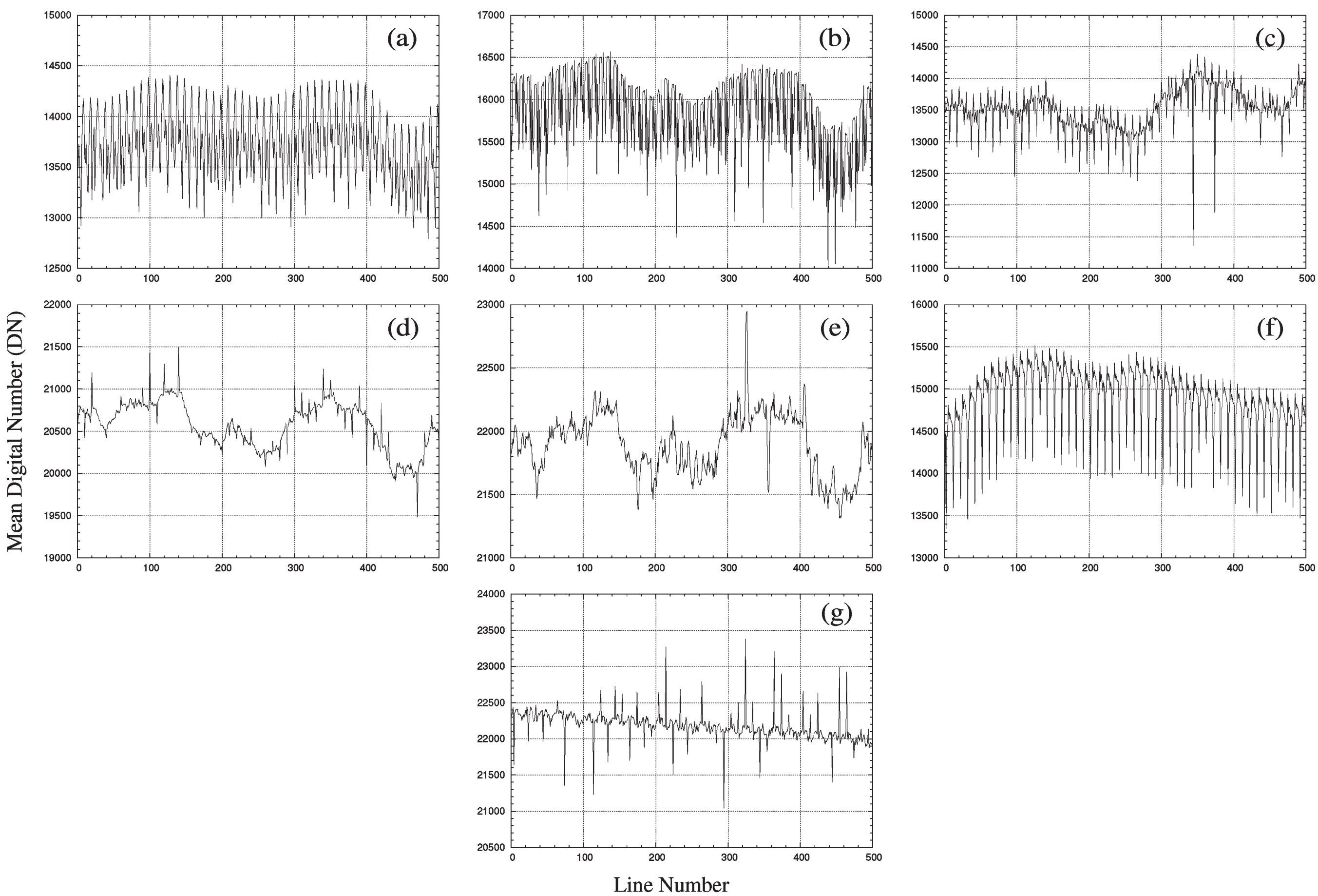

Fig. 9. Mean cross-track profiles of the along columns data extracted from Terra MODIS and Aqua MODIS images before noise reduction. Image sizes are sized 1354 × 500 pixels. Terra MODIS image was taken on September 16, 2004. Aqua MODIS image was taken on November 5, 2005. (a) Terra band 27, (b) Terra band 28, (c) Terra band 30, (d) Terra band 33, (e) Terra band 34, (f) Aqua band 27, and (g) Aqua band 36.

Therefore, the slope plane coefficients for each W_{ik} cell are calculated from

$$\alpha_{ik} = \frac{3}{L(L+1)(2L+1)^2} \sum_{r=-L}^{L} r \sum_{c=-L}^{L} g_{ik}(r,c) \tag{16}$$

$$\beta_{ik} = \frac{3}{L(L+1)(2L+1)^2} \sum_{c=-L}^{L} c \sum_{r=-L}^{L} g_{ik}(r,c) \tag{17}$$

$$\gamma_{ik} = \frac{1}{(2L+1)^2} \sum_{r=-L}^{L} \sum_{c=-L}^{L} g_{ik}(r,c). \tag{18}$$

In the case of the prediction of gray values of pixel i being covered by k resolution cells, there are k predicted values for pixel i given by $\hat{g}_{i1}, \hat{g}_{i2}, \ldots, \hat{g}_{iK\times K}$, where each prediction value has least-squares errors given by $\rho_{i1}, \rho_{i2}, \ldots,$

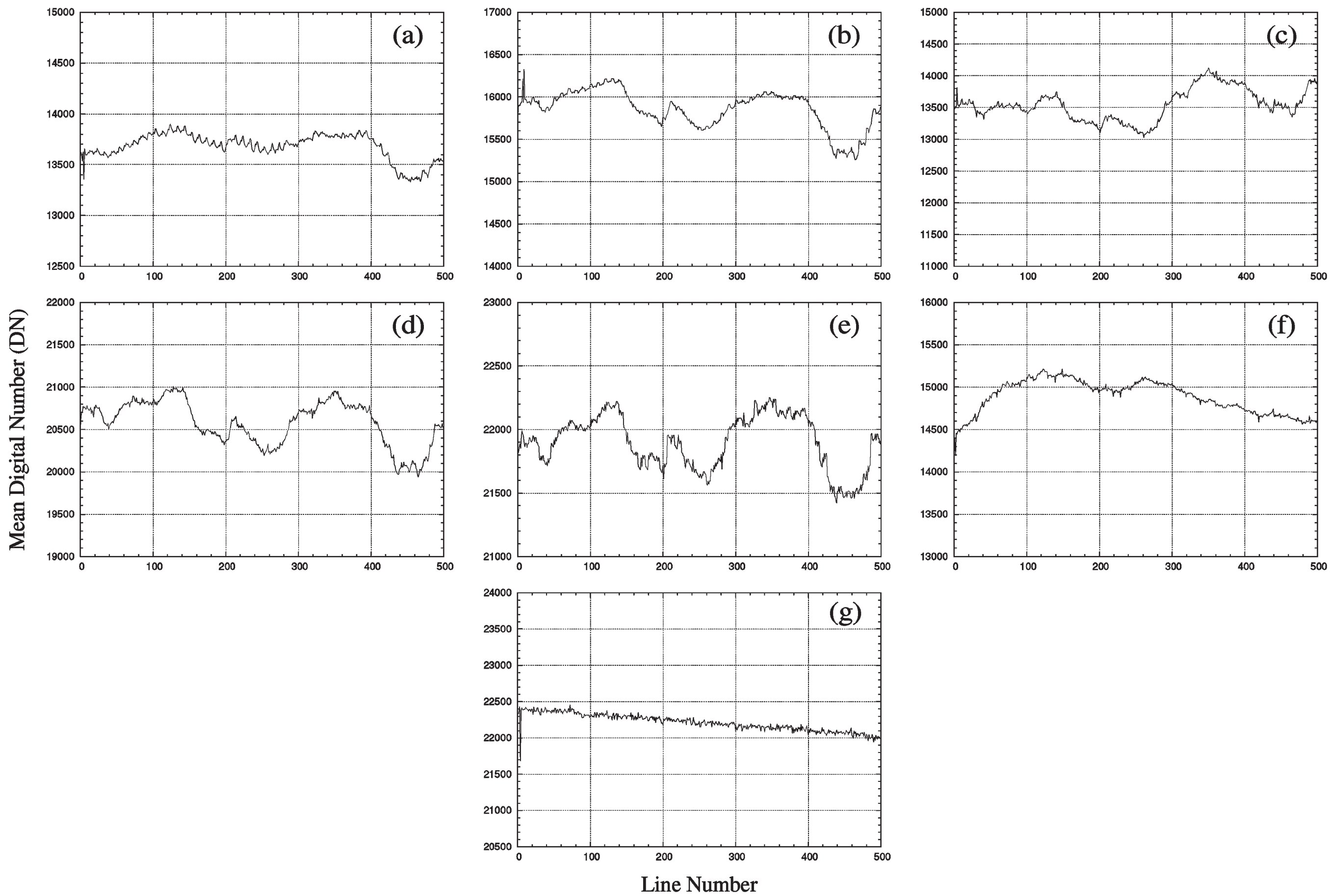

Fig. 10. Analogous to Fig. 9, except after destriping.

$\rho_{iK\times K}$, respectively. Least-squares errors can be calculated from

$$\rho_{ik} = \sum_{r=-L}^{L}\sum_{c=-L}^{L} \left(\hat{g}_{ik}(r,c) - g_{ik}(r,c)\right)^2, \qquad k=1,\ldots,K\times K. \tag{19}$$

Li and Tam [31] predict the gray values using the iterated WLS procedure given by

$$g_i^{(t+1)} = \sum_{k=1}^{K\times K} w_{ik}\hat{g}_{ik}^{(t)}, \qquad \text{where } w_{ik} = \frac{\rho_{ik}^{-1}}{\sum_{k=1}^{K\times K}\rho_{ik}^{-1}} \tag{20}$$

where $g_i^{(t+1)}$ is the gray value of the ith pixel at the $(t+1)$th iteration. Iteration in this paper means the repetition of the facet-filtering process. The weights w_{ik} are selected to be proportional to $1/\rho_{ik}$.

The neighborhood shape does not have to be square. Its size can be increased to an arbitrary K points. Li and Tam [31] mentioned that to improve the performance of noise filtering, it can be done by increasing the size of the facets at the expense of losing the resolution of fine detail in the image.

IV. Data Processing

In this research, Terra MODIS and Aqua MODIS data were obtained from the Institute of Industrial Science (IIS), University of Tokyo, on a direct broadcasting system. The original level 0 data are converted to level 1B data by International MODIS/AIRS Processing Package software (version 1.5) developed by the University of Wisconsin. Level 1B data are in hierarchical data format-EOS format, which is the standard data format of Terra and Aqua MODIS sensors. MODIS data are in the form of 12-bit precision brightness counts and coded to a 16-bit scale. MODIS images are freely available on the Web at http://webmodis.iis.u-tokyo.ac.jp/.

To determine the detectors contaminated by random noise, it is assumed that the first row of the original image is produced by the first detector of MODIS sensor. Therefore, MODIS data can be separated into ten subimages due to the ten rows of scan detectors. Fig. 2 shows the ten detector subimages of Terra MODIS band 28 taken on September 16, 2004. Each detector subimage has 200 pixels $\times$ 200 pixels and has been enhanced by histogram equalization to highlight the random noise of each detector. The noisy detectors were identified by visual interpretation. From Fig. 2, it can be seen that the image of Terra MODIS band 28 taken on September 16, 2004, has its noisy detectors in the first, second, third, seventh, eighth, and tenth detectors. When viewed along the vertical direction, the noise varies rapidly. The variation and amplitude of each detector

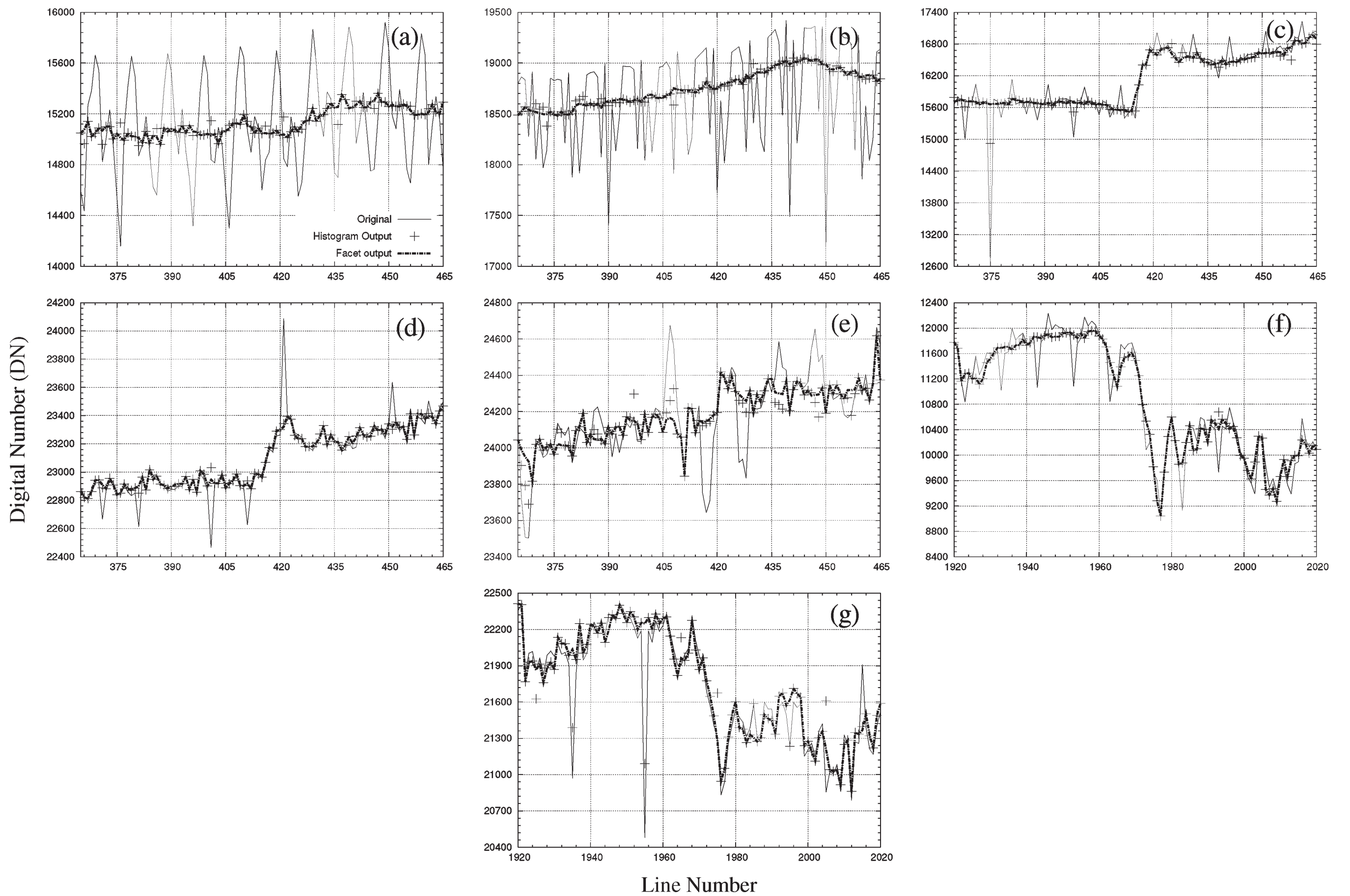

Fig. 11. DN value of profiles across the image data [shown in Fig. 4(c) and Fig. 5(a)] compare the original value with histogram-matching output and facet-filter output. Terra MODIS image was taken on September 16, 2004. Aqua MODIS image was taken on November 5, 2005. (a) Terra band 27, (b) Terra band 28, (c) Terra band 30, (d) Terra band 33, (e) Terra band 34, (f) Aqua band 27, and (g) Aqua band 36.

are varying independently. Fig. 2(h) and (j) shows the large variation in noise strength that occurs for the eighth and tenth detectors. Fig. 3 compares the pixels along the line of Terra MODIS band 28 taken on September 16, 2004. When viewed along the horizontal direction, the noise is almost coherent at different gain and offset [12].

For destriping, MODIS data are treated as 20 detectors because this corresponds to two sets of ten detectors, one for each mirror side. The CDF of each detector is adjusted to match the CDF of a reference detector (a nonnoisy detector). The lines contaminated by random noise are destriped again using an addition step created by Wegener [26]. The lines defected by random noise are divided into smaller size length 104 pixels. The length was determined after several tests. If the contaminated subline meets the Bienaymè's inequality criterion, its CDF is modified to the CDF of the neighbor subline that is not defected by this noise. Hereafter, the iterated weighted facet filter is used to remove the random noise from the line effected by this noise. After several adaptation tests for facet window size, a 5×3 window was selected where length is 5 pixels and width is 3 pixels since the noise is contaminated in the horizontal direction. This research uses three iterations as recommended by [31]. In total, the lines contaminated by random are processed 3 times—by histogram matching, Wegener method, and facet filter.

V. Result and Discussion

More than 20 MODIS scenes were analyzed in this paper. Tested scenes were taken in different seasons and locations. However, this paper used only the data received from IIS receiving station which has the coverage area ranging from the Pacific Ocean to Inner Mongolia. As an example of the results acquired from the proposed method, this paper selects the whole image data of Terra MODIS received on September 16, 2004 (1354×2030 pixels), and Aqua MODIS received on November 5, 2005 (1354×3110 pixels). The Terra MODIS scene used in this paper covers northern China and some part of the Korea peninsula. The Aqua MODIS scene covers some parts of Russia, the Korea peninsula, and Japan. This paper presents only the destriping results of MODIS bands that are contaminated by random noise. These are bands 27, 28, 30, 33, and 34 of Terra MODIS, and band 27 and band 36 of Aqua MODIS. Noisy detectors and their central wavelengths of Terra MODIS and Aqua MODIS bands are shown in Table I.

All images shown in this paper have been enhanced by histogram equalization in order to emphasize the striping appearance. Figs. 4 and 5 show strong striping in original subsets of the Terra MODIS and Aqua MODIS images sized 400×400 pixels. Figs. 6 and 7 show the improvement of overall data quality after applying the proposed destriping algorithm. Fig. 8

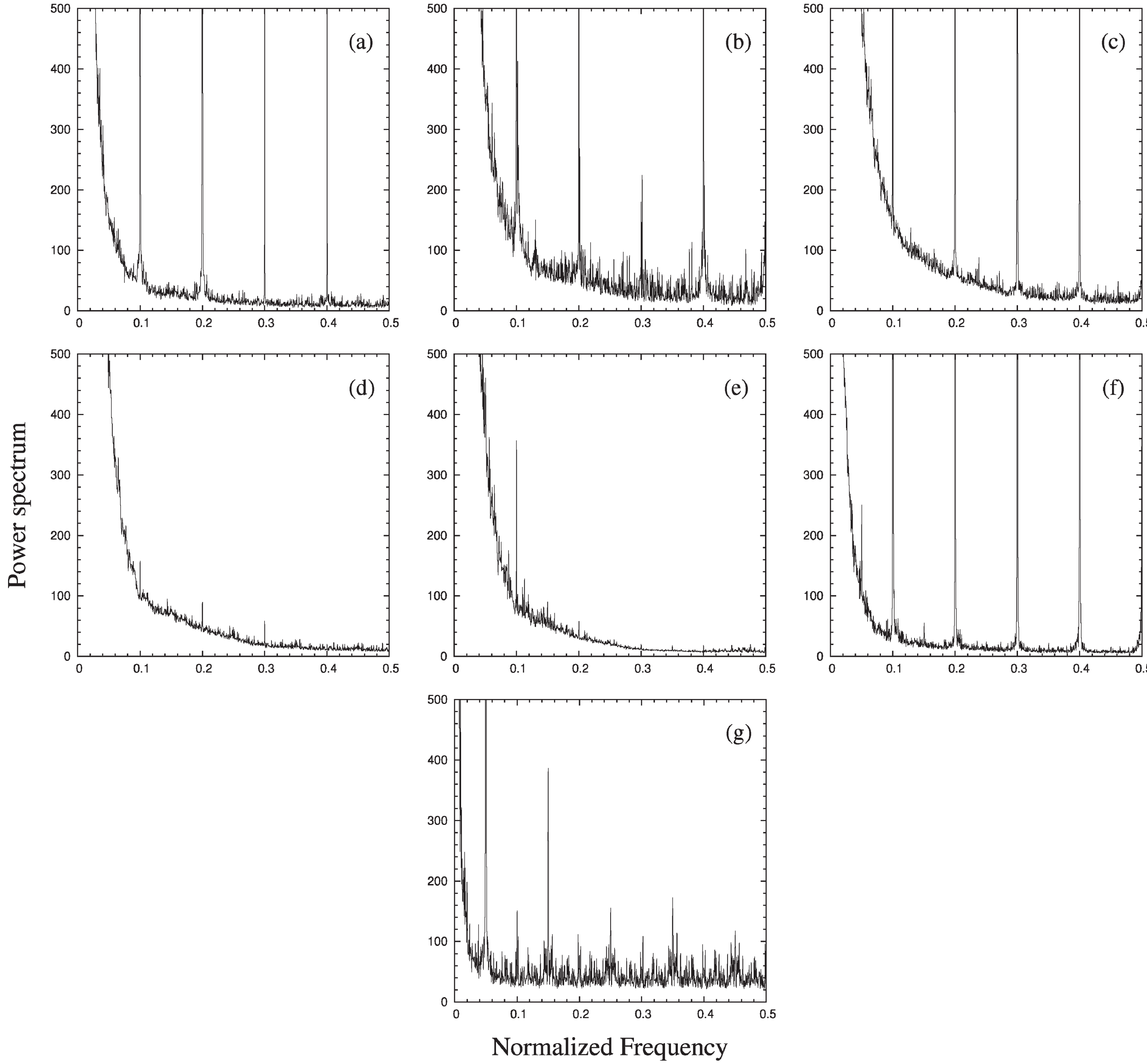

Fig. 12. Mean column power spectrum of the original Terra MODIS and Aqua MODIS images sized 1354 × 2030 pixels. Terra MODIS image was taken on September 16, 2004. Aqua MODIS image was taken on November 5, 2005: (a) Terra band 27, (b) Terra band 28, (c) Terra band 30, (d) Terra band 33, (e) Terra band 34, (f) Aqua band 27, and (g) Aqua band 36.

shows destriped results of the subimage of Terra MODIS band 30 using a low-pass filter, moment matching, and histogram matching without facet filtering, respectively. Even though the low-pass filter [Fig. 8(a)] can remove random noise, it causes significant blurring in the MODIS image. Moment matching [Fig. 8(b)] and histogram matching [Fig. 8(c)] improve the overall image quality, but stripe and random noises remain in the images.

Figs. 9 and 10 compare the mean cross-track profiles between MODIS images before and after destriping. It can be seen that the magnitude to the cross-track profiles of images before destriping vary randomly at the constant frequency of occurrence. After noise reduction, mean cross-track profiles of the images show the same change as the original images. These show the significant reduction of rapid fluctuations caused by stripe noises.

Fig. 11 shows the profiles of the lines shown in Figs. 4(c) and 5(a). The plots show the sharp transitions between land and sea of Terra MODIS and between cloud and cloud-free of Aqua MODIS. This demonstrates that the procedure has indeed removed stripe noises without altering the position of the real boundaries in the images.

Figs. 12 and 13 show the Fourier transforms of the test images both before and after destriping. The spectral shown in these images is ensemble-averaged power spectrum computed across the rows of the scene and plotted as a function of normalized frequency. For better visualization of noise reduction by the proposed method, very high spectral magnitudes are not

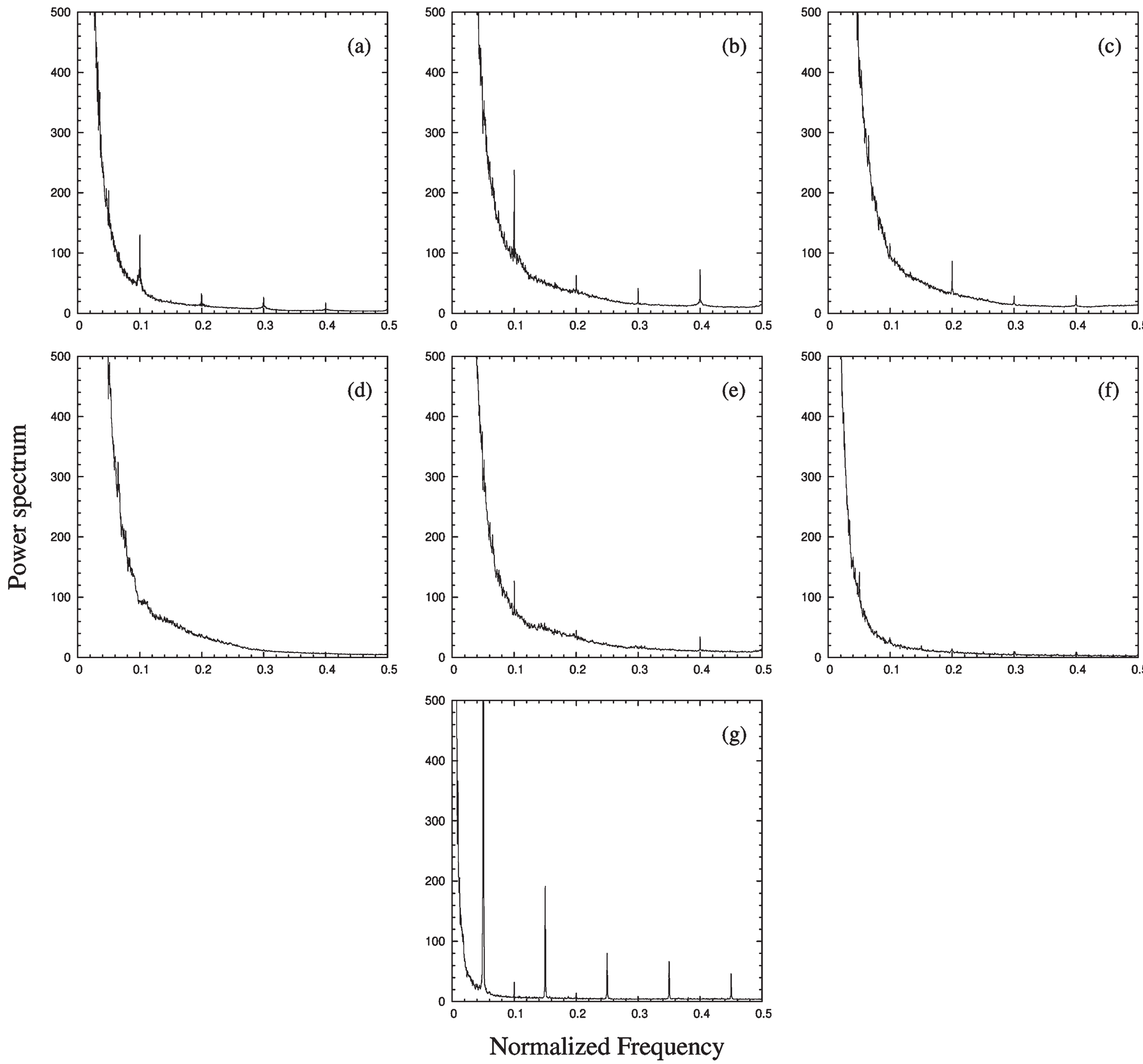

Fig. 13. Analogous to Fig. 12, except after destriping.

plotted. This provides a better range for the frequency components of the spectrum, where the noise is located. The inputs of the fast Fourier transform (FFT) were 2030 row vectors. The FFT produces 1015 spectral estimates.

Fig. 13 clearly shows that the pulses in the frequency domain, which are contaminated by the detector-to-detector stripes and mirror side stripes, are strongly reduced by the proposed method in this paper. The detector-to-detector stripe noise in Terra MODIS and Aqua MODIS images is narrowband at the frequencies of 1/10, 2/10, 3/10, 4/10, and 5/10 cycles per pixel. If a mirror side stripe occurs in the image, its pulses are located at the frequencies of 1/20, 3/20, 5/20, 7/20, and 9/20 cycles per pixel. Fig. 13(g) shows that the power of the frequency component contaminated by banding remains relatively high after destriping. This is because banding that occurred in these channels is correlated to the scan angle. Furthermore, Fig. 12 shows that the frequency components that are not affected by striping are also contaminated by random noise. By comparing Figs. 12 and 13, random noise superimposed on the frequency response was removed by the iterated WLS facet filter.

For quantitative measurement, two quality indexes are performed. These are ratio of noise reduction and inverse coefficient of variation (ICV), defined hereafter. The single steps of the algorithm 1) original image, 2) histogram-matching output, and 3) facet-filtering output are separately analyzed in order to investigate the different effects and the effectiveness of the reduction of each source of noise.

Noise reduction ratio was used in [13] and [15], and it is calculated from

$$\text{noise reduction} = \frac{N_\mathrm{o}}{N_\mathrm{k}} \tag{21}$$

TABLE II
MEAN VALUE, STANDARD DEVIATION, AND NOISE REDUCTION RATIO OF THE ORIGINAL MODIS DATA, HISTROGRAM-MATCHING OUTPUT, AND FACET-FILTER OUTPUT. TERRA MODIS IMAGE WAS TAKEN ON SEPTEMBER 16, 2004, AND AQUA MODIS IMAGE WAS TAKEN ON NOVEMBER 5, 2005

Band	Destriping step	Mean Value	Standard Deviation	NR
Terra B27	Original	15913	4089.13	1.00
	Histogram Output	15897	4135.08	233.10
	Facet Output	15894	4135.53	295.27
Terra B28	Original	17987	4290.91	1.00
	Histogram Output	18006	4312.43	210.47
	Facet Output	18004	4306.16	232.04
Terra B30	Original	14830	3107.20	1.00
	Histogram Output	14834	3084.30	45.60
	Facet Output	14834	3081.62	78.36
Terra B33	Original	21487	3336.35	1.00
	Histogram Output	21490	3335.67	1.70
	Facet Output	21488	3337.00	2.27
Terra B34	Original	22820	2999.40	1.00
	Histogram Output	2985.13	3335.67	1.73
	Facet Output	22814	2983.24	2.50
Aqua B27	Original	13335	2271.13	1.00
	Histogram Output	13335	2224.34	567.07
	Facet Output	13337	2224.46	880.86
Aqua B36	Original	21694	769.46	1.00
	Histogram Output	21731	689.89	0.27
	Facet Output	21731	688.88	7.06

where N_{o} stands for the power of the frequency components produced by stripe noise in the original image, and N_{k} stands for the power of the frequency components produced by stripe noise in the destriped images. Stripe noise components of the spectrum can be calculated by

$$N_i = \sum_{\mathrm{BW}_N} P_i(D) \tag{22}$$

where $P_i(D)$ is the averaged power spectrum down the columns of an image (where D is the distance from the origin in Fourier space); BW_N is the stripe noise region of the spectrum; $D \in \{0.1, 0.2, 0.3, 0.4, 0.5\}$ for detector-to-detector striping with addition $D \in \{0.05, 0.15, 0.25, 0.35, 0.45\}$ if there is mirror side striping. These noise reduction results are reported in Table II.

ICV was used in [32] and [33]. In this research, ICV is calculated for two 10×10 pixels homogeneous areas within the image. It can be calculated as follows:

$$\mathrm{ICV} = \frac{R_{\mathrm{a}}}{R_{\mathrm{sd}}} \tag{23}$$

where R_{a} refers to the signal response of a homogeneous surface and is calculated by averaging the pixels within a window of a given size; R_{sd} is referred to the noise components estimated by calculating the standard deviation of the pixel within the window. ICV results are given in Tables III and IV.

TABLE III
ICVs OF THE ORIGINAL TERRA MODIS DATA, HISTOGRAM-MATCHING OUTPUT AND FACET-FILTER OUTPUT. TERRA MODIS IMAGE WAS TAKEN ON SEPTEMBER 16, 2004. R_{a} = MEAN DIGITAL NUMBER WITHIN TEN PIXELS BY TEN PIXELS WINDOW. R_{sd} = STANDARD DEVIATION OF DN WITHIN THIS WINDOW

Band	Area	Before/After Destriping	R_a	R_{sd}	ICV
Terra B27	Sample 1	Original	15642	421.06	37.15
		Histogram Output	15686	97.40	161.04
		Facet Output	15685	95.20	164.76
	Sample 2	Original	15998	366.63	43.63
		Histogram Output	15988	131.33	121.74
		Facet Output	15983	127.75	125.11
Terra B28	Sample 1	Original	18627	442.75	42.07
		Histogram Output	18612	76.51	243.27
		Facet Output	18597	62.52	297.44
	Sample 2	Original	19008	614.22	30.95
		Histogram Output	19200	72.06	266.44
		Facet Output	19206	51.44	373.41
Terra B30	Sample 1	Original	15494	188.78	82.08
		Histogram Output	15496	55.41	279.64
		Facet Output	15514	41.29	375.69
	Sample 2	Original	16389	143.38	114.31
		Histogram Output	16342	49.73	328.64
		Facet Output	16348	44.41	368.08
Terra B33	Sample 1	Original	22741	173.32	131.21
		Histogram Output	22702	72.77	311.95
		Facet Output	22688	52.06	435.83
	Sample 2	Original	23063	114.26	201.85
		Histogram Output	23033	45.13	510.37
		Facet Output	23031	44.80	514.03
Terra B34	Sample 1	Original	24050	426.55	56.38
		Histogram Output	23824	93.85	253.85
		Facet Output	23811	61.12	389.55
	Sample 2	Original	24104	115.65	208.43
		Histogram Output	24049	81.43	295.35
		Facet Output	24059	59.88	401.78

VI. CONCLUSION

This paper presents a method to reduce the effect of stripe noises to both Terra MODIS and Aqua MODIS data. Detector-to-detector stripes, mirror side stripes, and noisy stripes can be overcome by using the combination of histogram matching with the iterated WLS facet filter. Histogram matching is used for reducing detector-to-detector stripes and mirror stripes. The iterated WLS facet algorithm is used for reducing noisy stripe. There are some MODIS products that could benefit from this destriping such as the MODIS cloud product (MOD06) and MODIS atmosphere product (MOD07). Finally, it is worth to mention that this method tries to reduce the striped noises through relative calibration and filtering. It is not meant to provide a radiometric correction. For this reason, it may create problems when applied to band data that will be used in numerical analysis. However, it may provide advantages

TABLE IV
ICVS OF THE ORIGINAL AQUA MODIS DATA, HISTOGRAM-MATCHING OUTPUT AND FACET-FILTERING OUTPUT. AQUA MODIS IMAGE WAS TAKEN ON NOVEMBER 5, 2005. R_{a} = MEAN DIGITAL NUMBER WITHIN TEN PIXELS BY TEN PIXELS WINDOW. R_{sd} = STANDARD DEVIATION OF DN WITHIN THIS WINDOW

Band	Area	Before/After Destriping	R_a	R_{sd}	ICV
Aqua B27	Sample 1	Original	11201	609.00	18.39
		Histogram Output	11208	450.50	24.88
		Facet Output	11312	76.00	148.85
	Sample 2	Original	12111	325.42	37.22
		Histogram Output	12106	117.57	102.97
		Facet Output	12130	93.65	129.53
Aqua B36	Sample 1	Original	21981	249.84	87.98
		Histogram Output	21940	140.73	155.90
		Facet Output	21969	100.10	219.48
	Sample 2	Original	22379	339.13	65.99
		Histogram Output	22267	116.80	190.65
		Facet Output	22267	108.93	204.41

for some processing. For instance, it may increase uniformity within spectral class, leading to improve the result of image classification.

ACKNOWLEDGMENT

The authors would like to thank the Ministry of Education, Culture, Sports, Science and Technology, Japan Government for the Ph.D. scholarship.

REFERENCES

[1] W. L. Barnes, T. S. Pagano, and V. V. Salomonson, "Prelaunch characteristics of the Moderate Resolution Imaging Spectroradiometer (MODIS) on EOS-AMl," *IEEE Trans. Geosci. Remote Sens.*, vol. 36, no. 4, pp. 1088–1100, Jul. 1998.
[2] B. Guenther, G. D. Godden, X. Xiong, E. J. Knight, S. Y. Qiu, H. Montgomery, M. M. Hopkins, M. G. Khayat, and Z. Hao, "Prelaunch algorithm and data format for the level 1 calibration products for the EOS-AM1 Moderate Resolution Imaging Spectroradiometer (MODIS)," *IEEE Trans. Geosci. Remote Sens.*, vol. 36, no. 4, pp. 1142–1151, Jul. 1998.
[3] B. Guenther, X. Xiong, V. V. Salomonson, W. L. Barnes, and J. Young, "On-orbit performance of the Earth observing system Moderate Resolution Imaging Spectroradiometer; first year of data," *Remote Sens. Environ.*, vol. 83, no. 1/2, pp. 16–30, Nov. 2002.
[4] Z. Wan, "Estimate of noise and systematic error in early thermal infrared data of the Moderate Resolution Imaging Spectroradiometer (MODIS)," *Remote Sens. Environ.*, vol. 80, no. 1, pp. 47–54, Apr. 2002.
[5] W. L. Barnes, X. Xiong, and V. V. Salomonson, "Status of Terra MODIS and Aqua MODIS," *Adv. Space Res.*, vol. 32, no. 11, pp. 2099–2106, 2003.
[6] X. Xiong, W. L. Barnes, B. Guenther, and R. E. Murphy, "Lessons learned from MODIS," *Adv. Space Res.*, vol. 32, no. 11, pp. 2107–2112, Dec. 2003.
[7] X. Xiong, N. Z. Che, and W. L. Barnes, "Terra MODIS on-orbit spatial characterization and performance," *IEEE Trans. Geosci. Remote Sens.*, vol. 43, no. 2, pp. 355–365, Feb. 2005.
[8] L. Gumley, *Proc. MODIS Workshop*, Nov. 26–29, 2002. URL: Western Australian Satellite Technology and Applications Consortium.
[9] R. Srinivasan, M. Cannon, and J. White, "Landsat data destriping using power filtering," *Opt. Eng.*, vol. 27, no. 11, pp. 939–943, 1988.
[10] R. E. Crippen, "A simple spatial filtering routine for the cosmetic removal of scan-line noise from Landsat TM P-tape imagery," *Photogramm. Eng. Remote Sens.*, vol. 55, no. 3, pp. 327–331, 1989.
[11] J. J. Pan and C. I. Chang, "Destriping of Landsat MSS images by filtering techniques," *Photogramm. Eng. Remote Sens.*, vol. 58, no. 10, pp. 1417–1423, Oct. 1992.
[12] J. J. Simpson and S. R. Yhann, "Reduction of noise in AVHRR channel 3 data with minimum distortion," *IEEE Trans. Geosci. Remote Sens.*, vol. 32, no. 2, pp. 315–328, Mar. 1994.
[13] J. J. Simpson, J. I. Gobat, and R. Frouin, "Improve destriping of GOES images using finite impulse response filters," *Remote Sens. Environ.*, vol. 52, no. 1, pp. 15–35, Apr. 1995.
[14] J. J. Simpson, J. R. Stitt, and D. M. Leath, "Improved finite impulse response filters for enhanced destriping of geostationary satellite data," *Remote Sens. Environ.*, vol. 66, no. 3, pp. 235–249, Dec. 1998.
[15] J. S. Chen, Y. Shao, H. D. Guo, W. Wang, and B. Zhu, "Destriping CMODIS data by power filtering," *IEEE Trans. Geosci. Remote Sens.*, vol. 41, no. 9, pt. 2, pp. 2119–2124, Sep. 2003.
[16] J. Torres and S. O. Infante, "Wavelet analysis for the elimination of striping noise in satellite images," *Opt. Eng.*, vol. 40, no. 7, pp. 1309–1314, Jul. 2001.
[17] Z. D. Yang, J. Li, W. P. Menzel, and R. A. Frey, "Destriping for MODIS data via wavelet shrinkage," in *Proc. SPIE—Applications with Weather Satellites*, 2003, vol. 4895, pp. 187–199.
[18] J. S. Chen, H. Lin, Y. Shao, and L. M. Yang, "Oblique striping removal in remote sensing imagery based on wavelet transform," *Int. J. Remote Sens.*, vol. 27, no. 8, pp. 1717–1723, Apr. 2006.
[19] G. Corsini, M. Diani, and T. Walzel, "Striping removal in MOS-B data," *IEEE Trans. Geosci. Remote Sens.*, vol. 38, no. 3, pp. 1439–1446, May 2000.
[20] P. Antonelli, M. di Bisceglie, R. Episcopo, and C. Galdi, "Destriping MODIS data using IFOV overlapping," in *Proc. IGARSS*, 2004, vol. 7, pp. 4568–4571.
[21] V. R. Algazi and G. E. Ford, "Radiometric equalization of nonperiodic striping in satellite data," *Comput. Graph. Image Process.*, vol. 16, no. 3, pp. 287–295, Jul. 1981.
[22] F. L. Gadallah and F. Csillag, "Destriping multidetector imagery with moment matching," *Int. J. Remote Sens.*, vol. 21, no. 12, pp. 2505–2511, 2000.
[23] B. K. P. Horn and R. J. Woodham, "Destriping Landsat MSS images by histogram modification," *Comput. Graph. Image Process.*, vol. 10, no. 1, pp. 69–83, 1979.
[24] D. J. Poros and C. J. Peterson, "Methods for destriping Landsat Thematic Mapper images—A feasibility study for an online destriping Landsat Thematic Mapper Image Processing System (TIPS)," *Photogramm. Eng. Remote Sens.*, vol. 51, no. 9, pp. 1371–1378, 1985.
[25] M. P. Weinreb, R. Xie, J. H. Lienesch, and D. S. Crosby, "Destriping GOES images by matching empirical distribution functions," *Remote Sens. Environ.*, vol. 29, no. 2, pp. 185–195, Aug. 1989.
[26] M. Wegener, "Destriping multiple detector imagery by improved histogram matching," *Int. J. Remote Sens.*, vol. 11, no. 5, pp. 859–875, 1990.
[27] D. L. Helder, B. Quirk, and J. Hood, "A technique for the reduction of banding in Landsat TM images," *Photogramm. Eng. Remote Sens.*, vol. 58, no. 10, pp. 1425–1431, 1992.
[28] D. L. Helder and B. K. Quirk, "Landsat Thematic Mapper reflective-band radiometric artifacts," *IEEE Trans. Geosci. Remote Sens.*, vol. 42, no. 12, pp. 2704–2716, Dec. 2004.
[29] R. M. Haralick and L. T. Watson, "A facet model for image data," *Comput. Graph. Image Process.*, vol. 15, no. 12, pp. 113–129, 1981.
[30] R. M. Haralick and L. G. Shapiro, *Computer and Robot Vision*. Reading, MA: Addison-Wesley, 1992.
[31] C. H. Li and P. R. S. Tam, "A global energy approach to facet model and its minimization using weighted least-squares algorithm," *Pattern Recogn.*, vol. 33, no. 2, pp. 281–293, Feb. 2000.
[32] G. M. Smith and P. J. Curran, "Methods for estimating image signal-to-noise ratio (SNR)," in *Advances in Remote Sensing and GIS Analysis*, P. M. Atkinson and N. J. Tate, Eds. Hoboken, NJ: Wiley, 2000, pp. 61–74.
[33] J. E. Nichol and V. Vohora, "Noise over water surfaces in Landsat TM images," *Int. J. Remote Sens.*, vol. 25, no. 11, pp. 2087–2094, Jun. 2004.

Preesan Rakwatin received the B.Eng. degree in electrical engineering from Kasetsart University, Bangkok, Thailand, in 1998, and the M.Eng. degree from the Asian Institute of Technology, Pathumthani, Thailand, in 2004. He is currently working toward the Ph.D. degree in civil engineering at the University of Tokyo, Tokyo, Japan.

His research interests include image processing and remote sensing.

Wataru Takeuchi received the B.Eng., M.Eng., and Ph.D. degrees in civil engineering from University of Tokyo, Tokyo, Japan, in 1999, 2001, and 2004, respectively.

He is currently an Assistant Professor at the Institute of Industrial Science, University of Tokyo. His research interests include agriculture remote sensing and image processing.

Yoshifumi Yasuoka (M'88–SM'89) received the B.Eng., M.Eng., and Ph.D. degrees in applied physics and mathematics from the University of Tokyo, Tokyo, Japan, in 1970, 1972, and 1975, respectively.

He was with the National Institute for Environmental Studies (NIES) from 1975 to 1998, serving as a Researcher, a Senior Researcher, and a Section Head in the Environmental Information Division. At the NIES, the last two years, he served as a Director of the Center for Global Environmental Research. In 1998, he moved to the University of Tokyo, and is currently a Professor at the Institute of Industrial Science, University of Tokyo. His major research fields are remote sensing, geographic information system, and spatial data analysis for environment and disaster assessment.

Dr. Yasuoka was a President of the Japan Remote Sensing Society from 2002 to 2004.